

Nucleon electromagnetic form factors using $N_f=2+1+1$ twisted mass fermion ensembles at the physical mass point

**C. Alexandrou,^{a,b} S. Bacchio,^b M. Constantinou,^c J. Finkenrath,^b
K. Hadjiyiannakou,^{a,b} K. Jansen,^d G. Koutsou^{b,*} and G. Spanoudes^b**

^a*Department of Physics, University of Cyprus, P.O. Box 20537, 1678 Nicosia, Cyprus*

^b*Computation-based Science and Technology Research Center, The Cyprus Institute, 20 Konstantinou Kavafi Str., 2121, Nicosia Cyprus*

^c*Temple University, 1801 N Broad Str., Philadelphia, PA 19122, USA*

^d*DESY-Zeuthen, 6 Platanenallee Str., 15738 Zeuthen, Germany*

E-mail: g.koutsou@cyi.ac.cy

We present results for the nucleon electromagnetic form factors using $N_f=2+1+1$ twisted mass lattice QCD with clover improvement and with quark masses tuned to their physical values. Our preliminary analysis includes three ensembles at similar physical volume and varying lattice spacing allowing us to take the continuum limit at the physical point. Both connected and disconnected contributions are evaluated, allowing us to take the isovector and isoscalar contributions as well as the individual proton and neutron form factors in the flavour isospin limit. For each ensemble we assess excited state effects using several sink-source time separations in the range 0.8 fm - 1.6 fm, exponentially increasing statistics with the separation.

*The 39th International Symposium on Lattice Field Theory (Lattice2022),
8-13 August, 2022
Bonn, Germany*

*Speaker

1. Introduction

The electromagnetic form factors of the nucleon are fundamental probes of its structure that map the charge distribution of its constituent quarks. Electron scattering experiments can provide a precise determination of the nucleon electromagnetic form factors with experiments, having been carried out since the fifties, continuing at experimental facilities at Mainz and JLab. In the limit of zero momentum transfer Q^2 , the slope of the electric, $G_E(Q^2)$, and magnetic, $G_M(Q^2)$, form factors is related to the electric and magnetic root mean square (rms) radii. Their value at $Q^2 = 0$ yields the electric charge and magnetic moment, respectively.

In this contribution, we present a calculation of the electromagnetic form factors of the nucleon using lattice QCD on three ensembles of twisted mass clover-improved twisted mass fermions with two degenerate light, strange, and charm quarks $N_f=2+1+1$ with masses tuned to their physical values (physical point). The three ensembles have similar physical spatial volume of $L^3 \simeq (5.5 \text{ fm})^3$ and different lattice spacings, namely $a = 0.08, 0.068, \text{ and } 0.057 \text{ fm}$, allowing for a continuum extrapolation at the physical point. Furthermore, calculation of the disconnected quark loop contributions allows the extraction of the individual proton and neutron form factors, as well as the strange form factors. Excited state effects are assessed using several sink-source time separations in the range $0.8 \text{ fm} - 1.6 \text{ fm}$, exponentially increasing statistics with the separation.

2. Lattice setup

2.1 Matrix elements

The Electromagnetic form factors are obtained from the matrix element of the vector operator O_μ^V :

$$\langle N(p', s') | O_\mu^V | N(p, s) \rangle = \sqrt{\frac{m_N^2}{E_N(\vec{p}')E_N(\vec{p})}} \bar{u}_N(p', s') \Lambda_\mu(q^2) u_N(p, s)$$

with $N(p, s)$ a nucleon state of momentum p and spin s , $E_N(\vec{p}) = p_0$ its energy and m_N its mass, u_N a nucleon spinor and, $q = p' - p$, the momentum transfer from initial (p) to final (p') momentum. The matrix element decomposes into the Dirac F_1 and Pauli F_2 form factors as follows,

$$\Lambda_\mu(q^2) = \gamma_\mu F_1(q^2) + \frac{i\sigma_{\mu\nu}q^\nu}{2m_N} F_2(q^2), \quad (1)$$

which can also be expressed in terms of the nucleon electric G_E and magnetic G_M Sachs form factors via $G_E(q^2) = F_1(q^2) + \frac{q^2}{(2m_N)^2} F_2(q^2)$ and $G_M(q^2) = F_1(q^2) + F_2(q^2)$.

2.2 Lattice extraction of form factors

On the lattice, the required matrix elements are obtained from combinations of two- and three-point correlation functions,

$$C(\Gamma_0, \vec{p}; t_s, t_0) = \sum_{\vec{x}_s} \text{Tr} [\Gamma_0 \langle J_N(x_s) \bar{J}_N(x_0) \rangle] e^{-i(\vec{x}_s - \vec{x}_0) \cdot \vec{p}} \quad \text{and} \quad (2)$$

$$C_\mu(\Gamma_\nu, \vec{p}, \vec{p}'; t_s, t_{\text{ins}}, t_0) = \sum_{\vec{x}_{\text{ins}}, \vec{x}_s} e^{i(\vec{x}_{\text{ins}} - \vec{x}_0) \cdot \vec{q}} e^{-i(\vec{x}_s - \vec{x}_0) \cdot \vec{p}'} \text{Tr} [\Gamma_\nu \langle J_N(x_s) j_\mu(x_{\text{ins}}) \bar{J}_N(x_0) \rangle] \quad (3)$$

respectively, with J the interpolating field of the nucleon, $x_0 = (t_0, \vec{x}_0)$ the *source*, j_μ the electromagnetic current, $x_{\text{ins}} = (t_{\text{ins}}, \vec{x}_{\text{ins}})$ the *insertion*, and $x_s = (t_s, \vec{x}_s)$ the *sink*. Γ_ν is a projector acting on spin indices, with $\Gamma_0 = \frac{1}{2}(1 + \gamma_0)$ and $\Gamma_k = \Gamma_0 i \gamma_5 \gamma_k$.

We form a ratio of three- to two-point functions [1] so as to cancel unknown overlaps and energy exponentials. The setup we use throughout is for the sink to be at rest ($\vec{p}' = 0$) which constrains $\vec{p} = -\vec{q}$ and for brevity we will stop from indicating the argument \vec{p}' . After taking the large time limit, the ratio yields the nucleon ground state matrix element, $\Pi_\mu(\Gamma_\nu; \vec{p})$, namely $R_\mu(\Gamma_\nu; \vec{p}; t_s; t_{\text{ins}}) \xrightarrow[t_{\text{ins}} \gg t_s - t_{\text{ins}}]{} \Pi_\mu(\Gamma_\nu; \vec{p})$. Since statistical errors increase exponentially with time separation, we cannot take t_{ins} and t_s arbitrarily large and, therefore, we evaluate the convergence to the ground state using the following methods:

- *Plateau method*: We identify a time-independent window (plateau) as a function of t_{ins} and fit to extract the plate value. We seek convergence of the plateau value as we increase t_s to extract the desired matrix element.
- *Two-state fit method*: We fit the two- and three-point functions considering contributions up to the first excited state, i.e. using the expressions

$$C(\vec{p}, t_s) = \sum_{i=0}^1 c_i(\vec{p}) e^{-\varepsilon_i(\vec{p}) t_s} \quad \text{and} \quad (4)$$

$$C_\mu(\Gamma_\nu, \vec{p}, t_s, t_{\text{ins}}) = \sum_{i,j=0}^1 A_{ij}^\mu(\Gamma_\nu, \vec{p}) e^{-E_i(0)(t_s - t_{\text{ins}}) - E_j(\vec{p}) t_{\text{ins}}}, \quad (5)$$

where A_{ij}^μ are proportional to the matrix element $\langle i | O_\mu | j \rangle$, with $|0\rangle$ and $|1\rangle$ denoting the ground and first excited state, E_0 and E_1 their energies, respectively, and $\varepsilon_0(\vec{p})$ and $\varepsilon_1(\vec{p})$ the ground and first excited state energies fitted from the two-point function. The desired matrix element is obtained via $\Pi_\mu(\Gamma_\nu; \vec{p}) = \frac{A_{00}^\mu(\Gamma_\nu, \vec{p})}{\sqrt{c_0(0)c_0(\vec{p})}}$. In our fitting procedure, we take the ground state to be the nucleon in both two- and three-point function, and therefore assume $E_0(0) = \varepsilon_0(0) = m_N$ and $E_0(\vec{p}) = \varepsilon_0(\vec{p}) = E_N = \sqrt{\varepsilon_0^2(0) + \vec{p}^2}$, but in general we make no assumptions this is the case for the excited state, i.e. $E_1(0) \neq \varepsilon_1(0)$ and $E_1(\vec{p}) \neq \varepsilon_1(\vec{p})$.

- *Summation method*: we sum the ratio over t_{ins} , [2, 3] which for large t_s yields: $R_\mu^{\text{sum}}(\Gamma_\nu; \vec{p}; t_s) = \sum_{t_{\text{ins}}} R_\mu(\Gamma_\nu; \vec{p}; t_s; t_{\text{ins}}) \xrightarrow[t_s \gg]{} c + t_s \Pi_\mu(\Gamma_\nu; \vec{p})$. We carry out a linear fit with t_s in order to extract the desired matrix element.

Having $\Pi_\mu(\Gamma; \vec{q})$, one can construct combinations of current insertion directions (μ) and projections Γ_μ to isolate the two form factors. Namely, we have:

$$\begin{aligned} \Pi_0(\Gamma_0; \vec{q}) &= C \frac{E_N + m_N}{2m_N} G_E(Q^2), & \Pi_i(\Gamma_k; \vec{q}) &= C \frac{\epsilon_{ijk} q_j}{2m_N} G_M(Q^2), & \text{and} \\ \Pi_i(\Gamma_0; \vec{q}) &= C \frac{q_i}{2m_N} G_E(Q^2), \end{aligned} \quad (6)$$

where $Q^2 = -q^2$, $C = \sqrt{\frac{2m_N^2}{E_N(E_N + m_N)}}$, and the projectors $\Gamma_0 = \frac{1 + \gamma_0}{4}$ and $\Gamma_k = i \gamma_5 \gamma_k \Gamma_0$, with $i, k = 1, 2, 3$.

2.3 Lattice setup and excited state analysis

We use three $N_f=2+1+1$ ensembles simulated using twisted mass clover-improved fermions as indicated in Table 1. Details on the simulation and scale setting for these ensembles can be found in Refs. [4] and [5]. For the connected contributions to the three-point correlation functions we analyze

Table 1: We show details of the ensembles analyzed, including their short name (first column), lattice volume (second column), lattice spacing in fm (third column), number of configurations analyzed (fourth column), sink-source separations (t_s/a) analyzed for the connected three-point functions with number of source positions per configuration (N_{src}) indicated as a subscript (fifth column), and number of source positions per configuration analyzed for the two-point function (N_{src}^{2p}).

Ens. ID	Vol.	a [fm]	N_{conf}	$(t_s/a)_{N_{\text{src}}}$	N_{src}^{2p}
cB64	64×128	0.080	750	8 ₁ , 10 ₂ , 12 ₄ , 14 ₆ , 16 ₁₆ , 18 ₄₈ , 20 ₆₄	264
cC80	80×160	0.068	400	6 ₁ , 8 ₂ , 10 ₄ , 12 ₁₀ , 14 ₂₂ , 16 ₄₈ , 18 ₄₅ , 20 ₁₁₆ , 22 ₂₄₆	600
cD96	96×192	0.057	500	8 ₁ , 10 ₂ , 12 ₄ , 14 ₈ , 16 ₁₆ , 18 ₃₂ , 20 ₆₄ , 22 ₁₆ , 24 ₃₂ , 26 ₆₄	368

multiple sink-source separations increasing the number of source-positions per configuration as indicated in Table 1. In addition, we have analyzed an increased number of statistics for the two-point functions, also indicated in Table 1, which are used to increase statistics for the disconnected contributions as well as to increase the robustness of the two-state fits. An example of the analysis carried out for the connected contributions is shown in Fig. 1 for the cC80 ensemble and considering one momentum transfer vector $\vec{q} = \frac{2\pi}{L}\vec{n}$, namely the first non-zero case $\vec{n}^2 = 1$. In particular we compare the summation method with three variants of the two-state fit method and observe that the fits in which we allow the electromagnetic three-point and the two-point functions to have different energies (crosses) yield large error-bars. Including the temporal component of the axial matrix element (A_0) as a third three-point function, motivated by Ref. [6] in which it was suggested this has high overlap with the π -N excited state contamination, yields more robust fits (filled circles) which are in tension to the results obtained when assuming the same spectrum in three- and two-point functions (open circles). In what follows we use the results for this variant of the two-state fit for the connected contributions.

For the disconnected quark loops, we use a combination of eigenvalue deflation [7], hierarchical probing [8], and spin and color dilution [9], as explained in Refs. [10–12]. For the connected electromagnetic form factors, we use the conserved vector current, which does not require renormalization, while for the disconnected case, we use the local vector current. The renormalization for the local vector current is carried out non-perturbatively in the RI'-MOM scheme [13] employing momentum sources, following the procedures described in Refs. [14, 15]. Details regarding the methods used for obtaining the disconnected contributions can be found in Refs. [10] and [11].

For the case of the disconnected contributions, the larger statistical errors do not allow fitting with the excited state energy different in two- and three-point function for all Q^2 values. Therefore, as shown in Fig. 2, we restrict to the summation and two-state fit method with $E_1(\vec{p}) = \varepsilon_1(\vec{p})$. As can be seen, the two methods agree and we take the summation method result for the disconnected in what follows.

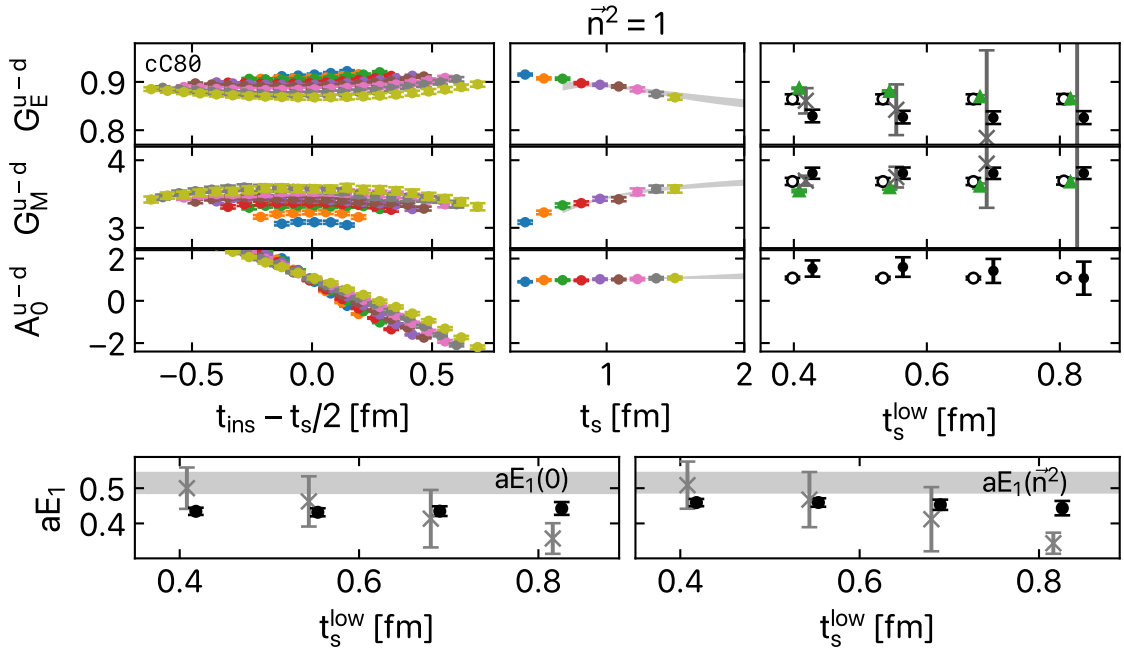


Figure 1: Example analysis of the isovector three-point function. Here we show the first non-zero momentum transfer for the cC80 ensemble. In the left column of the three first rows we show the ratios that yield G_E , G_M , and A_0 , indicating with different colors the different t_s/a (see Table 1). In the central column, we plot the plateau fits to each t_s and in the right column the summation method fits (green triangles) and two-state fits as a function of the smallest t_s entering the fit. The two-state fits are carried out i) assuming the same energies for the ground and first excited states in two- and three-point function (open circles), ii) allowing different energies between two- and three-point function (crosses), and iii) as in ii) but also including the fit to A_0 as an additional three-point function. In the bottom row we show the fitted excited state energy for both zero ($aE_1(0)$) and finite ($aE_1(\vec{n}^2)$) momentum as obtained from ii) and iii) while the bands denote the result from i).

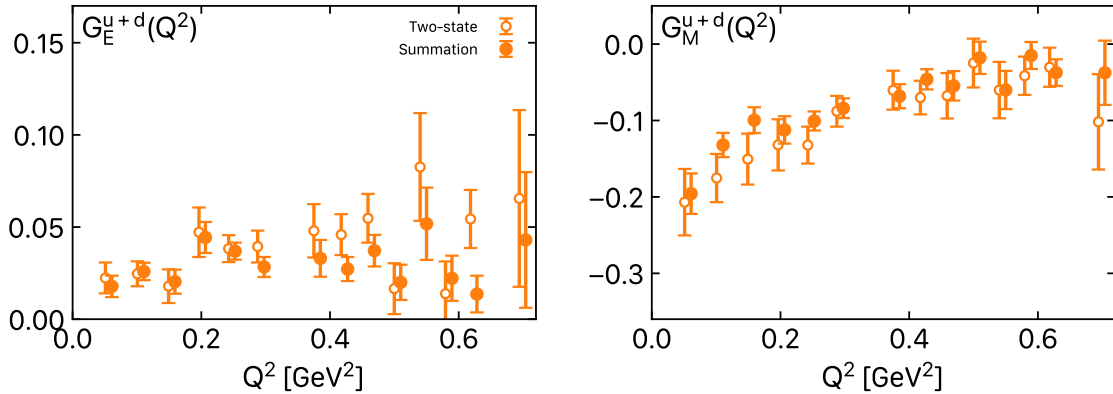


Figure 2: The disconnected contribution to the isovector electric (left) and magnetic (right) form factors as a function of the momentum transfer Q^2 for the cC80 ensemble. We compare results obtained using the summation method (filled circles) and the two-state fit method when taking the excited state energy in the two- and three-point function to be the same (open circles).

3. Results

Results for the isovector form factors and the disconnected contributions to the isoscalar form factors are summarized in Fig. 3 for the three ensembles listed in Table 1. To obtain our preliminary result for the continuum limit of the form factors, we carry out a linear interpolation in Q^2 of the data for the cB64 and cD96 ensembles to the Q^2 values of the cC80 ensemble, our intermediate lattice spacing. With the three ensembles at common Q^2 we carry out a linear extrapolation in a^2 to $a = 0$, also shown in Fig. 3. As can be seen in Fig. 3, the continuum extrapolation leads to lower values of the form factors, for both the electric and magnetic isovector form factors. Furthermore, the largest source of uncertainty in the continuum extrapolation is propagated from the coarsest ensemble, cB64, for which statistics are currently being increased.

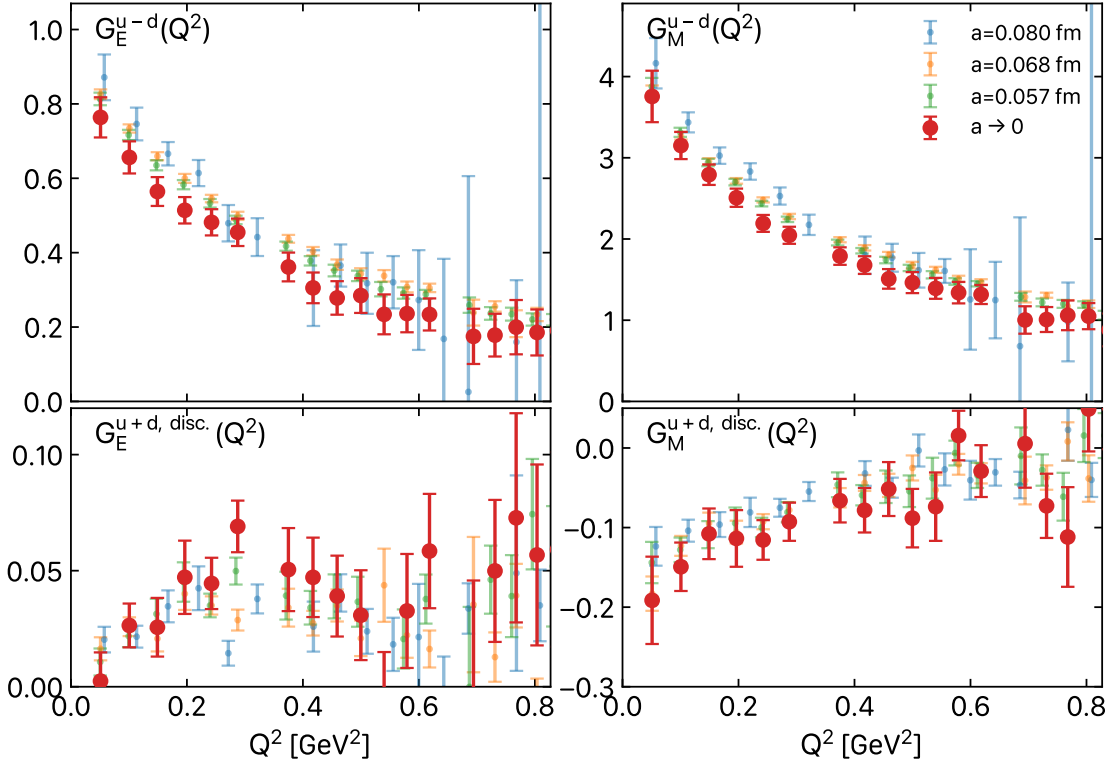


Figure 3: Isovector (top row) and disconnected contribution to the isoscalar (bottom row) electric (left) and magnetic (right) form factors of the nucleon. We show results for the cB64 (blue circles), cC80 (orange circles), and cD96 ensembles and a linear extrapolation to the continuum (red circles) as explained in the text.

Combining the isovector ($u - d$) and isoscalar ($u + d$) contributions, we obtain the individual proton and neutron electric (G_E^p and G_E^n respectively) and magnetic (G_M^p and G_M^n respectively) form factors in the flavor isospin limit via:

$$G_X^p = \frac{1}{6}G_X^{u+d} + \frac{1}{2}G_X^{u-d} \quad \text{and} \quad G_X^n = \frac{1}{6}G_X^{u+d} - \frac{1}{2}G_X^{u-d}, \quad (7)$$

with $X = E, M$. The results are shown in Fig. 4 where the same analysis as for the isovector is carried out to obtain the continuum limit.

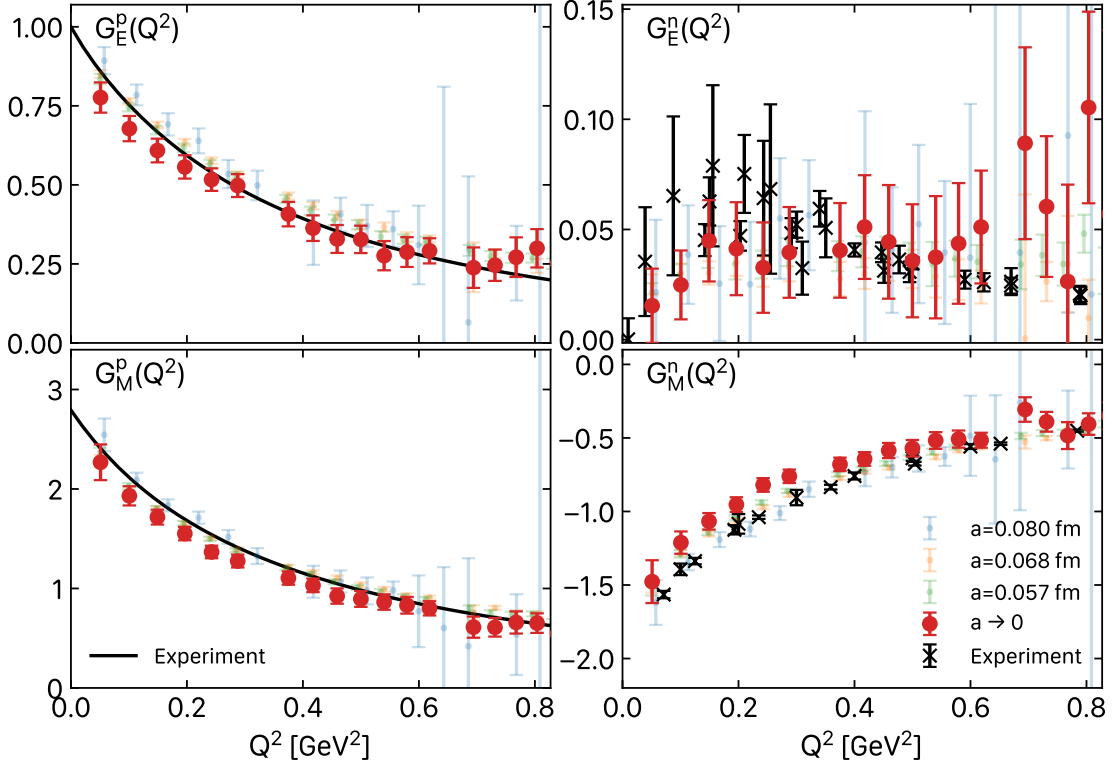


Figure 4: Electric (top row) and magnetic (bottom row) form factors of the proton (left) and neutron (right). The notation and the continuum extrapolation are as explained for Fig. 3. The experimental results are taken from Ref. [16], namely for the proton case we plot with the black curve their z -expansion fit [17] while for the neutron case we plot the quoted experimental data.

Comparing to the experimental results in Fig. 4, we see overall good agreement of our data. In particular, for this preliminary analysis where no systematic uncertainties have been estimated, we see that our results are at most 2σ away from the experimental results at small Q^2 values, while agreement is achieved within statistical errors for $Q^2 > 0.5 \text{ GeV}^2$.

4. Summary and outlook

We have carried out a preliminary analysis of the electromagnetic form factors of the nucleon using three ensembles of $N_f=2+1+1$ twisted mass fermions at three lattice spacings and with physical pion mass. For the coarsest of the ensembles, analysis has already been previously presented for the light [10] and strange [11] electromagnetic form factors. For the other two ensembles, this proceedings contribution shows results for the first time for these quantities. Connected contributions are calculated at multiple sink-source separations with increasing statistics and disconnected diagrams are calculated with an increased set of two-point functions. Excited state effects are analyzed using the summation method as well as the two-state fit method with variants that allow for a different first

excited state in the two- and three-point function. For the connected contributions, a robust analysis requires including the isovector temporal component of the axial form factor A_0^{u-d} to resolve a πN excited state in the electromagnetic three-point function.

We carry out a preliminary, linear continuum extrapolation in a^2 by interpolating the form factors to common values of Q^2 . Our continuum limit results, which for this preliminary study do not have quantified systematic uncertainties, are in general agreement when compared to experiment, with some tension not larger than 2σ for smaller values of Q^2 . Furthermore, in our analysis the major source of statistical error in the extrapolated form factors is due to the relatively larger statistical uncertainties in our coarsest ensemble. Analysis is under way to increase statistics for this ensemble, as well as for the larger separations of the finest ensemble (see Table 1).

With increased statistics, we will vary our method for obtaining the continuum limit to include allow for quantifying systematic uncertainties. Furthermore, future plans include extracting the electric and magnetic radii and magnetic moments at the continuum limit, which will be one of the first such calculations using only ensembles at the physical point.

Acknowledgments

We thank all members of the ETM collaboration for a most conducive cooperation. G.K. acknowledges support from projects NextQCD, NiceQuarks, and FAST co-funded by the European Regional Development Fund and the Republic of Cyprus through the Research and Innovation Foundation (RIF) (EXCELLENCE/0918/0129, EXCELLENCE/0421/0195, and COMPLEMENTARY/0916/0048). S.B., J.F., and G.S. are supported by the H2020 project PRACE 6-IP (GA No. 82376) and the EuroCC (GA No. 951740). K.H. is supported by RIF under contract no. POST-DOC/0718/0100. Partial support is provided by the Marie Skłodowska Curie joint doctorate program STIMULATE (GA No. 765048). We acknowledge the Gauss Centre for Supercomputing e.V. (www.gauss-centre.eu) for project pr74yo by providing computing time on SuperMUC at LRZ (www.lrz.de) and JUWELS-booster at the JSC (www.fz-juelich.de). This work used resources from NIC on JUWELS at the JSC, under projects with ids renormglue and tmdpdf1. We acknowledge PRACE for awarding us access to Marconi100 at CINECA within the project Pra24_0002.

References

- [1] ETM collaboration, *Axial Nucleon form factors from lattice QCD*, *Phys. Rev. D* **83** (2011) 045010 [[1012.0857](#)].
- [2] L. Maiani, G. Martinelli, M.L. Paciello and B. Taglienti, *Scalar Densities and Baryon Mass Differences in Lattice QCD With Wilson Fermions*, *Nucl. Phys. B* **293** (1987) 420.
- [3] S. Capitani, M. Della Morte, G. von Hippel, B. Jager, A. Juttner, B. Knippschild et al., *The nucleon axial charge from lattice QCD with controlled errors*, *Phys. Rev. D* **86** (2012) 074502 [[1205.0180](#)].
- [4] C. Alexandrou et al., *Simulating twisted mass fermions at physical light, strange and charm quark masses*, *Phys. Rev. D* **98** (2018) 054518 [[1807.00495](#)].

- [5] EXTENDED TWISTED MASS collaboration, *Quark masses using twisted-mass fermion gauge ensembles*, *Phys. Rev. D* **104** (2021) 074515 [2104.13408].
- [6] Y.-C. Jang, R. Gupta, B. Yoon and T. Bhattacharya, *Axial Vector Form Factors from Lattice QCD that Satisfy the PCAC Relation*, *Phys. Rev. Lett.* **124** (2020) 072002 [1905.06470].
- [7] A.S. Gambhir, A. Stathopoulos and K. Orginos, *Deflation as a Method of Variance Reduction for Estimating the Trace of a Matrix Inverse*, *SIAM J. Sci. Comput.* **39** (2017) A532 [1603.05988].
- [8] A. Stathopoulos, J. Laeuchli and K. Orginos, *Hierarchical probing for estimating the trace of the matrix inverse on toroidal lattices*, [1302.4018](#).
- [9] UKQCD collaboration, *Decay width of light quark hybrid meson from the lattice*, *Phys. Rev. D* **73** (2006) 074506 [hep-lat/0603007].
- [10] C. Alexandrou, S. Bacchio, M. Constantinou, J. Finkenrath, K. Hadjiyiannakou, K. Jansen et al., *Proton and neutron electromagnetic form factors from lattice QCD*, *Phys. Rev. D* **100** (2019) 014509 [1812.10311].
- [11] C. Alexandrou, S. Bacchio, M. Constantinou, J. Finkenrath, K. Hadjiyiannakou, K. Jansen et al., *Nucleon strange electromagnetic form factors*, *Phys. Rev. D* **101** (2020) 031501 [1909.10744].
- [12] C. Alexandrou, S. Bacchio, M. Constantinou, K. Hadjiyiannakou, K. Jansen and G. Koutsou, *Quark flavor decomposition of the nucleon axial form factors*, *Phys. Rev. D* **104** (2021) 074503 [2106.13468].
- [13] G. Martinelli, C. Pittori, C.T. Sachrajda, M. Testa and A. Vladikas, *A General method for nonperturbative renormalization of lattice operators*, *Nucl. Phys. B* **445** (1995) 81 [hep-lat/9411010].
- [14] C. Alexandrou, M. Constantinou, T. Korzec, H. Panagopoulos and F. Stylianos, *Renormalization constants for 2-twist operators in twisted mass QCD*, *Phys. Rev. D* **83** (2011) 014503 [1006.1920].
- [15] ETM collaboration, *Renormalization functions for $N_f=2$ and $N_f=4$ twisted mass fermions*, *Phys. Rev. D* **95** (2017) 034505 [1509.00213].
- [16] Z. Ye, J. Arrington, R.J. Hill and G. Lee, *Proton and Neutron Electromagnetic Form Factors and Uncertainties*, *Phys. Lett. B* **777** (2018) 8 [1707.09063].
- [17] R.J. Hill and G. Paz, *Model independent extraction of the proton charge radius from electron scattering*, *Phys. Rev. D* **82** (2010) 113005 [1008.4619].